

Spin-allowed and spin-forbidden $4f^n \leftrightarrow 4f^{n-1}5d$ transitions for heavy lanthanides in fluoride hosts

R. T. Wegh* and A. Meijerink

Debye Institute, Utrecht University, P.O. Box 80000, 3508 TA Utrecht, The Netherlands

(Received 17 May 1999)

Luminescence spectra of lanthanides in the vacuum ultraviolet spectral region have revealed interesting features for $4f^n \leftrightarrow 4f^{n-1}5d$ (f - d) transitions. For Tb^{3+} , Dy^{3+} , Ho^{3+} , Er^{3+} , and Tm^{3+} in $LiYF_4$, weak f - d bands are present in the excitation spectra at lower energy than the usually observed strong f - d bands. The weakness of the bands is explained by the spin-forbidden character of transitions from the $4f^n$ ground state to these $4f^{n-1}5d$ states. For Er^{3+} and Tm^{3+} , upon excitation in the higher energetic $4f^{n-1}5d$ states two kinds of f - d emission are observed: fast spin-allowed emission with a decay time in the order of ns, and slow spin-forbidden emission with a decay time in the order of μ s. These two types of f - d emission are also found for Er^{3+} and Tm^{3+} in other fluoride hosts. [S0163-1829(99)11239-6]

I. INTRODUCTION

In the past few years, optical spectroscopy of lanthanide ions in the vacuum ultraviolet spectral region (VUV; $\lambda < 200$ nm, $E > 50\,000$ cm $^{-1}$) has become an important field of research. The fact that the VUV spectroscopy of lanthanides has remained a largely unexplored region for decades is due to experimental difficulties and lack of applications. Especially the latter point has changed recently. New luminescent materials (phosphors) that emit visible light upon VUV excitation are required for mercury-free fluorescent lamps and plasma display panels (for flat TV's).^{1,2} In both cases, a noble gas discharge (e.g., xenon) generates VUV radiation, which has to be absorbed by the phosphors. For these applications, the intraconfigurational (parity-forbidden) $4f^n \leftrightarrow 4f^n$ transitions (further called f - f transitions) are of importance. We have investigated the previously unknown $4f^n$ energy levels in the VUV for a number of lanthanides and the possibilities to achieve visible quantum efficiencies higher than 100% upon VUV excitation.^{3,4} Next to $4f^n \leftrightarrow 4f^n$ transitions, knowledge and understanding of the interconfigurational $4f^n \leftrightarrow 4f^{n-1}5d$ (f - d) transitions is needed for several reasons. These transitions are parity allowed, and therefore suitable for efficient absorption of VUV radiation from the noble gas discharge in mercury-free lamps and plasma display panels. A well-known application of the strong f - d absorption of lanthanides is in blue lamp phosphors with Eu^{2+} , e.g., $BaMgAl_{10}O_{17}:Eu^{2+}$. Potential applications for which VUV f - d emission can be used are tunable VUV lasers and scintillator materials. The first solid-state VUV laser was based on the f - d emission of Nd^{3+} in LaF_3 .⁵ For scintillation crystals, the luminescence properties of Ce^{3+} are widely studied because of the short decay time of the f - d emission of Ce^{3+} (usually in the UV).⁶ Because of the success of Ce^{3+} -doped materials, investigation of the f - d emission of other lanthanides is interesting.⁶

In this paper, VUV f - d excitation and emission spectra for a number of trivalent lanthanides incorporated in fluorides are reported. We have found new features of the f - d transitions in these spectra, which were not noticed in previ-

ous papers. Already in 1966 the lowest f - d absorption bands for all trivalent lanthanide ions in CaF_2 were reported by Loh.⁷ Synchrotron radiation was used to study f - d transitions for the first time in the seventies.⁸ Later, high-resolution absorption spectra for all trivalent lanthanides in CaF_2 were presented by Szczurek and Schlesinger.⁹ Also other fluoride hosts, e.g. $LiYF_4$, LaF_3 , YF_3 , and BaY_2F_8 , have been used to investigate the f - d spectroscopy of a number of lanthanides in the VUV.¹⁰⁻¹⁸ An important feature, spin-forbidden f - d transitions, was overlooked in all these studies. In the high-resolution excitation spectra reported here for the lanthanides with a more than half-filled $4f$ shell, weak bands are observed at the longer-wavelength side of the well-known strong f - d bands. These weak bands are assigned to transitions to the lowest $4f^{n-1}5d$ state, which has a higher spin quantum number than the $4f^n$ ground state. As a consequence these transitions are spin forbidden, which explains its weakness in comparison to the previously observed fully allowed f - d bands. For Tb^{3+} ($4f^8$) this spin-forbidden transition has been observed (and assigned) a number of times, as it is situated in the UV.¹⁹⁻²¹ As far as we are aware, Jørgensen and Brinen were the first to assign the spin-forbidden f - d transition for $Tb(III)$ aqua ions.¹⁹ To the best of our knowledge, it was never reported before for Ln^{3+} with $n > 8$. In this paper, we report and discuss the presence of spin-forbidden f - d transitions for Tb^{3+} , Dy^{3+} ($4f^9$), Ho^{3+} ($4f^{10}$), Er^{3+} ($4f^{11}$), and Tm^{3+} ($4f^{12}$).

The existence of the high-spin $4f^{n-1}5d$ state has important consequences for the f - d luminescence of Er^{3+} and Tm^{3+} . Because the emission from the lowest $4f^{n-1}5d$ state is spin forbidden, the decay time is in the μ s range. Next to this slow spin-forbidden emission, fast spin-allowed emission from the higher-energetic $4f^{n-1}5d$ state with a decay time in the order of ns is observed. This situation is comparable with the phosphorescence and fluorescence occurring in organic molecules from the triplet and singlet state, respectively. These observations were reported by us before for Er^{3+} in $LiYF_4$.²² In this paper, the results are extended to other lanthanides with a more than half-filled $4f$ shell and to other host lattices.

II. EXPERIMENT

The doped LiYF_4 , YF_3 , and LaF_3 samples measured were polycrystalline powders or single crystals. In case a single crystal was used it is indicated in the text. The crystals were grown in a glassy carbon crucible using the vertical Bridgman method in a nitrogen atmosphere.³ To prevent oxygen contamination, the crystal-growth chamber was flushed with SF_6 for about 30 min during melting of the dry starting materials.²³ Polished, transparent pieces (typically $4 \times 4 \times 2$ mm) were used for the measurements. The powder samples were prepared either by conventional solid state techniques³ (only for LiYF_4 doped with Er^{3+} and Ho^{3+}), or by grinding of a crystalline sample obtained from the melt as described above. The concentration of the rare-earth dopant in the crystal-growth melt was 0.5, 1, or 2%. The phase purity of all samples was checked by x-ray diffraction analysis. LiYF_4 has the inverse scheelite structure with site symmetry S_4 for the lanthanide ion.²⁴ In YF_3 the site symmetry for the cation is C_s .²⁵

The experiments were performed at the DESY Synchrotron in Hamburg (Germany) using the HIGITI experimental station of HASYLAB. With this setup high-resolution excitation spectra in the range 100–250 nm were recorded. Emission spectra could be measured with either a channelplate detector (VUV/UV) or a photomultiplier tube (UV/visible). Reflectivity measurements in the VUV range were performed by scanning the excitation and VUV emission monochromator synchronously. Next to that, time-resolved measurements were carried out using a time-to-amplitude converter. An upper limit to the measuring range was imposed by the time between the positron bunches in the synchrotron. The bunch separation time was at maximum 1 μs (single bunch mode), which means that decay times of at maximum a few μs could be determined. The lower limit was approximately 100 ps, which is the time resolution of the multichannel plate. The temperature of the sample could be varied between 10 K and room temperature in a cold-finger liquid-helium cryostat. Further details on the setup are given elsewhere.³ Excitation spectra were corrected for the intensity of the synchrotron radiation and the transmission of the excitation monochromator.

For high-resolution excitation spectra around 250 nm an excimer-laser-pumped dye laser equipped with a frequency-doubling crystal was used. This setup consisted of a Lambda Physik LPD 3000 tunable dye laser, which was pumped by a Lambda Physik LPX 100 XeCl-excimer laser. The dye Coumarine 307 was used to obtain a tunable range from 490 to 520 nm, which was frequency-doubled by a Lambda Physik BBO1 crystal. The sample was cooled in an Oxford Instruments Optistat^{CF-V} liquid-helium cold-finger cryostat. The emission was detected with a Jobin Yvon HR 1000 monochromator and a cooled Hamamatsu R928 photomultiplier tube. The spectra were corrected for the excitation intensity as a function of wavelength by measuring the UV light output with a power meter.

III. RESULTS AND DISCUSSION

3.1. $f-d$ excitation for Ln^{3+} in LiYF_4

In Fig. 1(a), the $f-d$ excitation spectrum of $\text{LiYF}_4:\text{Tb}^{3+}$ is presented. The spectrum shows strong excitation bands at

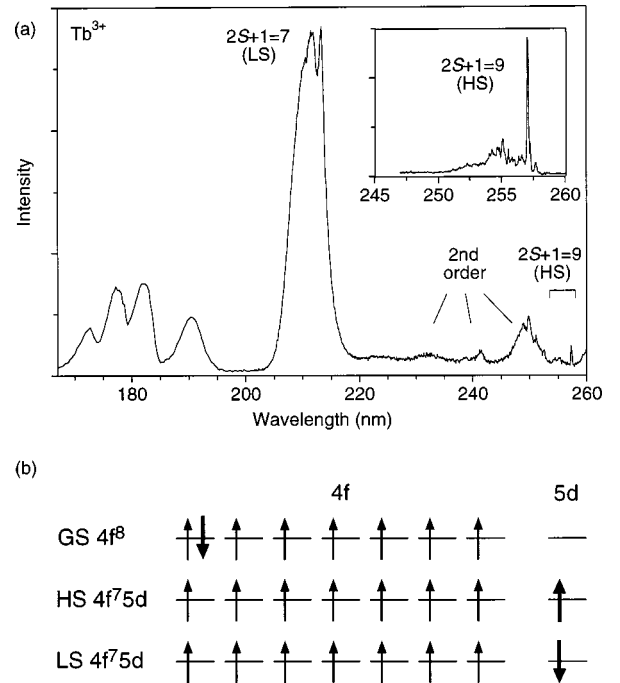


FIG. 1. (a) Excitation spectrum of $\text{LiYF}_4:\text{Tb}^{3+}$ 1% monitoring $4f^8(^5D_4 \rightarrow ^7F_5)$ emission (545 nm) at 10 K. Inset: high-resolution excitation spectrum monitoring $4f^8(^5D_4 \rightarrow ^7F_5)$ emission (545 nm) at 10 K, recorded with a tunable laser setup. (b) Schematic electron configurations for the ground state (GS), the lowest-energetic high-spin $4f^75d$ state (HS), and the higher-energetic low-spin $4f^75d$ state (LS) for Tb^{3+} .

211, 191, 182, 177, and 173 nm and several more at shorter wavelength (not shown), which are all assigned to $4f^8 \rightarrow 4f^75d$ ($f-d$) transitions on Tb^{3+} . It is similar to the excitation spectrum previously reported for Tb^{3+} in LiYF_4 .¹⁷ The $f-d$ excitation band at 211 nm consists of a zero-phonon line and a vibronic sideband. The observation of fine structure can be explained by the restricted relaxation in the excited $4f^{n-1}5d$ state due to the relatively weak electron-lattice coupling for lanthanides in LiYF_4 . The weak coupling manifests itself also in the fact that the $f-d$ excitation bands are relatively narrow. A similar fine structure has been reported before for Ce^{3+} in LiYF_4 .²⁶ A detailed discussion on the $4f^{n-1}5d$ structure of Tb^{3+} as well as other lanthanides in LiYF_4 will be given in a forthcoming paper.²⁷

At the longer-wavelength side of the band at 211 nm in Fig. 1(a), several weak bands are observed. Most of them can be assigned to second order bands of the Tb^{3+} $f-d$ excitations at 125, 120, and 116 nm.²⁷ The very weak band around 255 nm and the sharp line at 257 nm, however, cannot be assigned to second order excitations, since no excitations are present between 126 and 129 nm.²⁷ The inset of Fig. 1(a) shows a high-resolution excitation spectrum recorded with the laser setup. This spectrum proves that these features around 255 nm are indeed a first order excitation, since this spectrum can not contain second-order bands in this region, as there is no VUV excitation light. The sharp line at 257 nm and the band between 252 and 257 nm are assigned to a spin-forbidden $f-d$ transition. This assignment is explained with the schematic spin configuration diagrams in Fig. 1(b).

In the ground-state $4f^8$ configuration (GS), the maximum number of unpaired parallel spins is 6, which results in a total spin quantum number $S=3$ and therefore, a spin multiplicity $2S+1=7$. When one electron is promoted to the $5d$ shell, it can orient its spin in two ways: either parallel with the 7 remaining $4f$ electrons, giving rise to a high-spin state (HS) with $S=4$ and $2S+1=9$, or antiparallel, yielding a low-spin state (LS) with $S=3$ and $2S+1=7$. According to Hund's rule, the high-spin state will be lower in energy. Thus, the transition from the ground state to the lowest $4f^75d$ state will be spin forbidden and therefore, relatively weak compared to the higher-energy $f-d$ excitations, which are spin allowed. Based on these considerations, the sharp line at 257 nm and the weak band around 255 nm are assigned to the zero-phonon line and the vibronic sideband of the spin-forbidden $f-d$ transition, respectively.

Figures 2(a)–2(d) show the $f-d$ excitation spectra of LiYF_4 doped with Dy^{3+} ($4f^9$), Ho^{3+} ($4f^{10}$), Er^{3+} ($4f^{11}$), and Tm^{3+} ($4f^{12}$), respectively. The wavelength ranges displayed were chosen in such a way that in energy they are as wide as for $\text{LiYF}_4:\text{Tb}^{3+}$ in Fig. 1(a). The four spectra in Fig. 2 have a number of similarities. In all cases, several strong $f-d$ excitation bands are observed, some of which exhibit fine structure. Low-resolution spectra of the strong $f-d$ bands have been reported before for these lanthanides in LiYF_4 .^{10,17} In all four spectra weak bands are present at the longer-wavelength side, which all show vibrational structure very similar to that of the strong excitation bands. As Dy^{3+} , Ho^{3+} , Er^{3+} , and Tm^{3+} all have a more than half-filled $4f$ shell, a higher maximum number of unpaired parallel spins than in the ground state can be obtained when an electron is promoted to the $5d$ shell. Therefore, the bands around 184 and 193 nm for Dy^{3+} and around 163 nm for Ho^{3+} , Er^{3+} , and Tm^{3+} can all be assigned to $f-d$ transitions to the high-spin states, which are spin forbidden and thus weak. The spin multiplicities of the high-spin and low-spin $4f^{n-1}5d$ states to which the $f-d$ transitions observed take place are given in Fig. 2.

In the excitation spectrum of $\text{LiYF}_4:\text{Dy}^{3+}$ a broad band due to an impurity is observed between 187 and 200 nm. Therefore, an excitation spectrum in the region 175–200 nm obtained for a single crystal of $\text{LiYF}_4:\text{Dy}^{3+}$ is also given (inset). This spectrum shows that two similar weak bands are present, which are both assigned to spin-forbidden $f-d$ transitions. Although Dy^{3+} is the only lanthanide ion for which we have observed this, the presence of two (or more) spin-forbidden $f-d$ transitions at lower energy than the spin-allowed ones can occur. The $5d$ state is split by the crystal field in up to five levels, but because of interaction with the partially filled $4f$ shell, the number of $4f^{n-1}5d$ states is higher for lanthanides with $n>1$. For all these $4f^{n-1}5d$ states the spin of the electron in the $5d$ orbital can have two orientations, giving rise to a high-spin and a low-spin state. If the energy difference between the two lowest high-spin states is smaller than the difference between the lowest high-spin and low-spin state, two spin-forbidden $f-d$ transitions will be observed. Apparently, for Dy^{3+} in LiYF_4 this is the case. In the excitation spectrum shown in the inset also some weak sharp lines corresponding to $f-f$ transitions are observed. These will be discussed in a paper on the $4f^9$ levels of Dy^{3+} in the VUV.

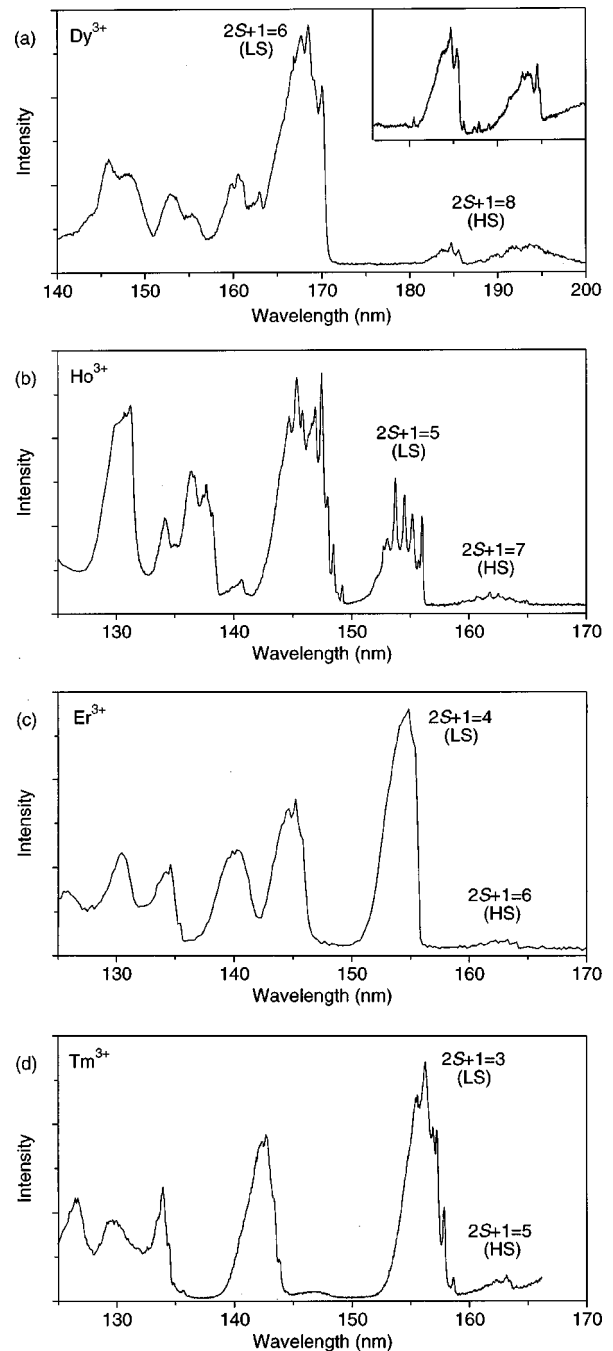


FIG. 2. (a) Excitation spectrum of $\text{LiYF}_4:\text{Dy}^{3+}$ 1% monitoring $4f^9(^4F_{9/2} \rightarrow ^6H_{13/2})$ emission (575 nm) at 10 K. Inset: Excitation spectrum of a 1% single-crystal sample monitoring all visible $4f^9 \rightarrow 4f^9$ emission at 9 K; the wavelength scale corresponds with the lower spectrum. (b) Excitation spectrum of $\text{LiYF}_4:\text{Ho}^{3+}$ 1% monitoring all visible $4f^{10} \rightarrow 4f^{10}$ emission at 9 K. (c) Excitation spectrum of $\text{LiYF}_4:\text{Er}^{3+}$ 2% monitoring $4f^{11}(^4S_{3/2} \rightarrow ^4I_{15/2})$ emission (551 nm) at 10 K. (d) Excitation spectrum of $\text{LiYF}_4:\text{Tm}^{3+}$ 1% monitoring $4f^{11}5d(\text{HS}) \rightarrow 4f^{12}(^3H_6)$ emission (170 nm) at 12 K. The sloping curve towards longer wavelengths is due to stray light.

The present observation of spin-forbidden $f-d$ transitions for heavy lanthanides could be expected in analogy with the results reported 30 years ago for Tb^{3+} .^{19–21} It is surprising that they have not been reported before to our knowledge. In fact, a careful analysis of $f-d$ spectra of the heavier trivalent lanthanides in a few publications shows that the weak bands

corresponding to spin-forbidden $f-d$ transitions can be observed. However, the weak bands were either not understood because of the intermediate oscillator strength between $f-f$ and $f-d$ transitions^{11,12} and therefore erroneously ascribed to interactions between lanthanide ions,¹¹ or no attention was given to them.^{16,17}

For the light lanthanides ($n \leq 7$) no weak spin-forbidden $f-d$ transitions at lower energy than the strong $f-d$ bands are expected. In the $4f^n$ ground state all $4f$ electron spins are parallel, so the maximum number of parallel spins can not be higher for the $4f^{n-1}5d$ state. As a consequence, the spin multiplicity for the lowest-energetic $4f^{n-1}5d$ state will be the same as for the ground state. In agreement with this expectation, we have observed sharp onsets for the first strong $f-d$ excitation bands for $\text{Ce}^{3+}(4f^1)$, $\text{Pr}^{3+}(4f^2)$, $\text{Nd}^{3+}(4f^3)$, and $\text{Sm}^{3+}(4f^5)$, and no weak spin-forbidden $f-d$ bands are present on the longer-wavelength side.²⁷ For $\text{Yb}^{3+}(4f^{13})$ a weak spin-forbidden $f-d$ excitation band just as for the other heavy lanthanides can be expected. Nevertheless, it cannot be observed as the $f-d$ excitations are obscured by the charge transfer transition, which is situated at lower energy.²⁸

The excitation measurements shown in this section were performed on powder samples, because for single crystals the relative intensities of the $f-d$ bands change and the fine structure is obscured. This can be explained by saturation of the strong $f-d$ excitation transitions, which plays a role in the single crystals due to the longer optical path length compared to powder samples.²⁹ Most of the emission measurements on Er^{3+} and Tm^{3+} in LiYF_4 , which will be treated in the next section, were performed on single crystals.

3.2. $f-d$ emission for Er^{3+} and Tm^{3+} in LiYF_4

Figure 3(a) shows the low-temperature emission spectrum in the VUV/UV region of Er^{3+} in LiYF_4 upon excitation into one of the higher-lying low-spin $4f^{10}5d$ states. In this spectrum a number of emission bands are present, which are all assigned to $f-d$ transitions. For proper assignment of these bands, a close up of the excitation and emission spectrum in the region 140–180 nm is given in Fig. 3(b). This excitation spectrum was recorded with a higher resolution than the spectrum in Fig. 2(c), and therefore, more fine structure is observed. In the emission spectra no fine structure can be seen. This is due to the rather poor resolution of the VUV/UV emission monochromator (1 nm at best). The strong emission band at 167 nm is assigned to the transition from the high-spin $4f^{10}5d$ state (sextet state) to the $4f^{11}$ ground state $^4I_{15/2}$. The Stokes shift is about $1.5 \times 10^3 \text{ cm}^{-1}$, which is a relatively small value for an $f-d$ transition. This is due to the weak electron-lattice coupling and is similar to values measured for $f-d$ emission from other lanthanides in LiYF_4 .^{13,26} At longer wavelengths the emission bands corresponding to transitions from the sextet $4f^{10}5d$ state to $^4I_{13/2}$ (186 nm), $^4I_{11/2}$ (198 nm), $^4I_{9/2}$ (208 nm), $^4F_{9/2}$ (225 nm), and $^4S_{3/2}$ (244 nm) can also be observed. However, the emission bands at 159 and 176 nm cannot be assigned to transitions from the sextet state. As can be seen in Fig. 3(b), the 159-nm emission band is shifted some $1.5 \times 10^3 \text{ cm}^{-1}$ to lower energy relative to the lowest spin-allowed $f-d$ excitation band. This shift is approximately

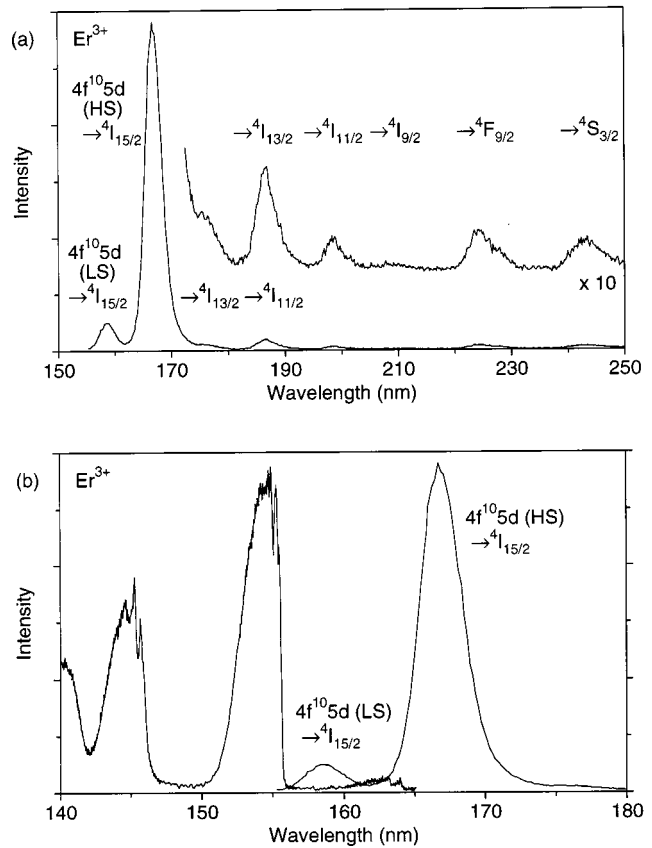


FIG. 3. (a) Emission spectrum of $\text{LiYF}_4:\text{Er}^{3+}$ 2% (single crystal) upon $4f^{11}(^4I_{15/2}) \rightarrow 4f^{10}5d$ excitation (140 nm) at 7 K. (b) Closeup of the excitation (left, $\lambda_{em} = 551 \text{ nm}$) and emission (right, $\lambda_{exc} = 140 \text{ nm}$) spectra of $\text{LiYF}_4:\text{Er}^{3+}$ at 10 K.

equal to the Stokes shift for the $4f^{10}5d(\text{HS}) \rightarrow 4f^{11}(^4I_{15/2})$ emission, and therefore the 159-nm emission band is assigned to the transition from the low-spin $4f^{10}5d$ state (quartet state) to the $^4I_{15/2}$ ground state. The weak band at 176 nm is assigned to the emission from the quartet $4f^{10}5d$ state to the $^4I_{13/2}$ multiplet of Er^{3+} .

The schematic configurational coordinate diagram in Fig. 4 illustrates this situation. Upon excitation in the low-spin $4f^{10}5d$ states of Er^{3+} , there are two competing decay processes: either $f-d$ emission from the lowest-energetic quartet $4f^{10}5d$ state occurs, or nonradiative decay to the sextet $4f^{10}5d$ state occurs, which is also called intersystem crossing. From the sextet state $f-d$ emission takes place, which is spin forbidden and thus expected to be slow. The emission from the higher-lying quartet $4f^{10}5d$ state is spin allowed and therefore relatively fast, so that it can compete with nonradiative decay. In addition, nonradiative relaxation from the quartet to the sextet state is hampered by the fact that one electron spin has to change its orientation. That this is essential for the occurrence of emission from the low-spin $4f^{10}5d$ state, is illustrated by a comparison with the $f-d$ emission of Ce^{3+} in LiYF_4 . Although the energy difference between the two lowest $5d$ states of Ce^{3+} (some $7 \times 10^3 \text{ cm}^{-1}$) (Ref. 30) is much larger than the energy difference between the low-spin and high-spin $4f^{10}5d$ states of Er^{3+} , upon excitation in the higher $5d$ states of Ce^{3+} only emission from the lowest-

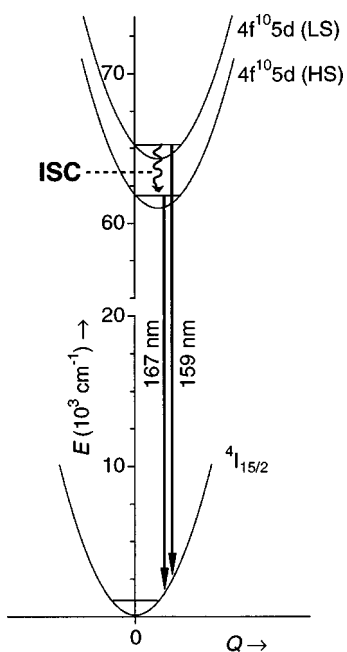


FIG. 4. Configurational coordinate diagram for Er^{3+} in LiYF_4 explaining the observed f - d emission bands. ISC=intersystem crossing. Note the break in the energy scale.

$5d$ level is observed. The efficient nonradiative relaxation is due the fact that the $5d$ states of Ce^{3+} all have the same spin multiplicity ($2S+1=2$).

The situation for Er^{3+} is very similar to the luminescence behavior in organic molecules after $\pi \rightarrow \pi^*$ excitation. From the singlet excited state, either fast (spin-allowed) emission to the singlet ground state can occur (fluorescence), or intersystem crossing to the lower-lying triplet excited state can occur, which is followed by slow (spin-forbidden) emission (phosphorescence). The presently observed f - d luminescence provides an inorganic analog of this well-known observation of fluorescence and phosphorescence in organic systems.

To provide further evidence that the model in Fig. 4 is correct, three experiments were performed: selective excitation and emission spectra, luminescence decay curves, and time-resolved emission spectra were recorded. Selective excitation spectra monitoring emission at 176 nm, which was assigned to spin-allowed f - d emission, and 186 nm, which is mainly spin-forbidden emission, are given in Fig. 5 (upper and lower curve, respectively). In agreement with the model, in the excitation spectrum of the 176-nm emission band only the spin-allowed f - d excitation band at 154 nm is present. The absence of the weak excitation band around 163 nm shows that this emission cannot be excited in the sextet $4f^{10}5d$ state. Note that the background increase towards longer wavelengths is caused by scattered excitation light close to the monitored emission wavelength. In the excitation spectrum of the 186-nm emission band both spin-allowed and spin-forbidden f - d excitation bands are observed, as expected. The feature at 158 nm may be due to excitation to the $4f^{11}$ level ${}^2F(2)_{5/2}$, which is located at this energy.²⁷ Next to these excitation spectra, we recorded an emission spectrum for selective excitation into the sextet $4f^{10}5d$ state at

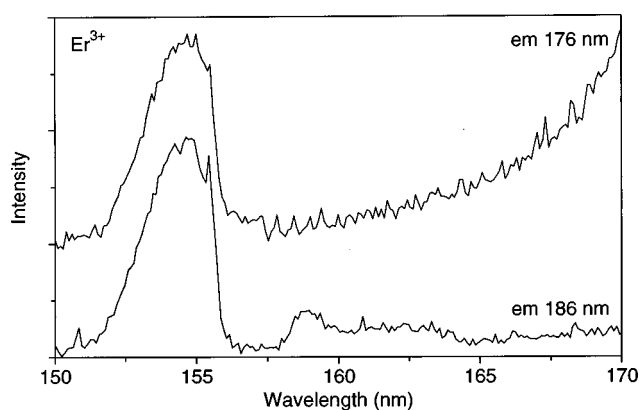


FIG. 5. Selective excitation spectra for $\text{LiYF}_4:\text{Er}^{3+}$ 0.5% monitoring the spin-allowed $4f^{10}5d(\text{LS}) \rightarrow 4f^{11}({}^4I_{13/2})$ emission at 176 nm (upper curve) and the spin-forbidden $4f^{10}5d(\text{HS}) \rightarrow 4f^{11}({}^4I_{13/2})$ emission at 186 nm (lower curve), both at 10 K. The sloping increase towards longer wavelengths in the upper curve is due to stray light.

162 nm. In this spectrum, not shown here, the spin-allowed emission band at 176 nm originating from the quartet $4f^{10}5d$ state is absent. The luminescence decay curves recorded for the 159 and 167 nm emission band are shown in Figs. 6(a) and 6(b), respectively. The decay curve of the 159-nm band is clearly single-exponential and a decay time of 4.5 ns was obtained, which is in agreement with the spin-allowed (and parity-allowed) character of this transition. For the 176-nm emission band the same decay time was measured as for the

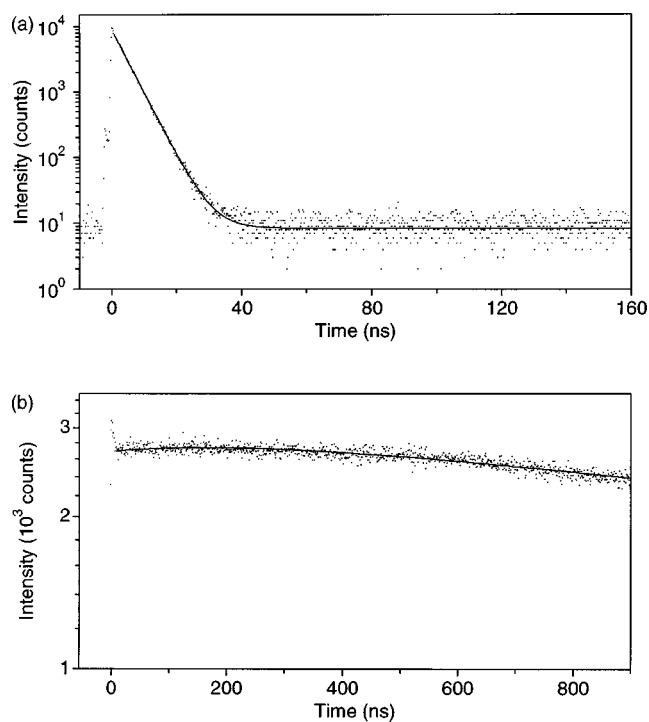


FIG. 6. Luminescence decay curves for $\text{LiYF}_4:\text{Er}^{3+}$ 2% (single crystal) of (a) the spin-allowed $4f^{10}5d(\text{LS}) \rightarrow 4f^{11}({}^4I_{15/2})$ emission at 159 nm and (b) the spin-forbidden $4f^{10}5d(\text{HS}) \rightarrow 4f^{11}({}^4I_{15/2})$ emission at 167 nm, both at 10 K. The dots form the experimental curve, the line is the fit curve. Note the different scaling of both intensity and time.

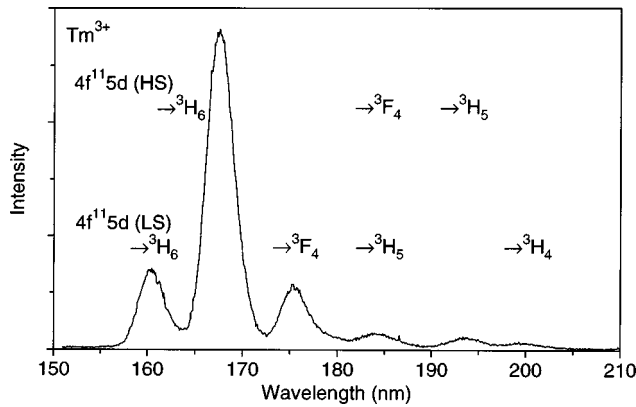


FIG. 7. Emission spectrum of $\text{LiYF}_4:\text{Tm}^{3+}$ 1% (single crystal) upon $4f^{12}(^3H_6) \rightarrow 4f^{11}5d$ excitation (143 nm) at 7 K.

159-nm emission, so these emissions indeed originate from the same state. The decay curve of the 167-nm emission band in Fig. 6(b) was recorded in the maximum time range of 1 μs . It is clear that the curve decreases slightly within this time period, which indicates that the decay time of this emission is in the μs range. It can also be seen that the curve is not single exponential: a rise time of the order of a few tenths of a μs is present. This rise time has the following origin. As was mentioned above, Er^{3+} has a $4f^{11}$ level [$^2F(2)_{5/2}$] at about $63\,300\text{ cm}^{-1}$ above the ground state (158 nm), which is in between the sextet and the quartet $4f^{10}5d$ state [see Figs. 2(c) and Fig. 4]. Upon excitation in the quartet $4f^{10}5d$ states of Er^{3+} in LiYF_4 , nonradiative decay to the sextet state proceeds via this $^2F(2)_{5/2}$ level. We have found that in $\text{LiYF}_4:\text{Er}^{3+}$, next to spin-allowed and spin-forbidden $f-d$ emission, also emission from the $^2F(2)_{5/2}$ state occurs. This $f-f$ emission, which will be treated in detail in another paper,²⁷ has a decay time of some tenths of a μs , depending on temperature. The initial rise in the decay curve of the 167-nm emission band corresponds with this value, as the sextet $4f^{10}5d$ state is fed by the decay from the $^2F(2)_{5/2}$ state. Taking this into account, a decay time of 3 μs was obtained from a double-exponential curve fit. This relatively long decay time agrees with the assignment of the 167-nm emission band to a spin-forbidden transition.

Finally, time-resolved emission spectra for the $\text{LiYF}_4:\text{Er}^{3+}$ 2% single-crystalline sample were recorded upon excitation into the $4f^{10}5d$ state at 140 nm at low temperature (not shown). In the spectrum obtained using a time gate of 5 ns and no delay, the 167-nm band, which was assigned to a spin-forbidden (slow) emission, has nearly vanished relative to the 159-nm band. The emission at 176 nm, only a shoulder in Fig. 3(a), is clearly present in this spectrum detecting only fast emission. The emission spectrum obtained using a delay of about 100 ns and a gate of about 350 ns shows a very strong 167-nm band. The 159- and 176-nm bands are absent. All these observations confirm the assignments to spin-allowed and spin-forbidden $f-d$ emissions.

The emission spectrum of $\text{LiYF}_4:\text{Tm}^{3+}$ for $f-d$ excitation, which is shown in Fig. 7, is similar to the $f-d$ emission spectrum of $\text{LiYF}_4:\text{Er}^{3+}$ [Fig. 3(a)]. This is not surprising because for Tm^{3+} in LiYF_4 the lowest low-spin and high-spin $4f^{10}5d$ states are situated at the same positions as for

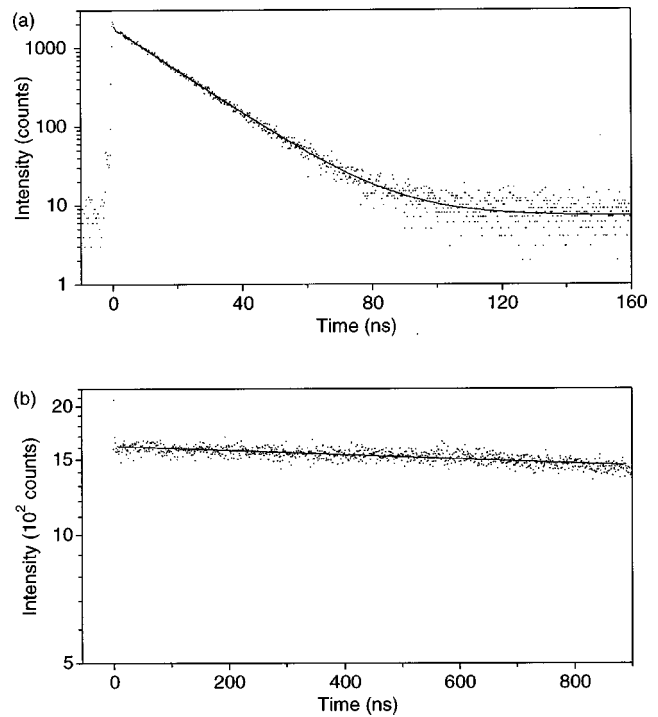


FIG. 8. Luminescence decay curves for $\text{LiYF}_4:\text{Tm}^{3+}$ 1% (single crystal) of (a) the spin-allowed $4f^{11}5d(\text{LS}) \rightarrow 4f^{12}(^3H_6)$ emission at 161 nm and (b) the spin-forbidden $4f^{11}5d(\text{HS}) \rightarrow 4f^{12}(^3H_6)$ emission at 168 nm, both at 10 K. The dots form the experimental curve, the line is the fit curve. Note the different scaling of both intensity and time.

Er^{3+} (Sec. 3.1). The strongest emission band in Fig. 7 at 168 nm corresponds to the transition from the high-spin $4f^{11}5d$ state (quintet state) to the $4f^{12}$ ground state 3H_6 , and is therefore spin forbidden. The spin-forbidden emissions from the quintet $4f^{11}5d$ state to the 3F_4 and 3H_5 multiplets are observed at 184 and 194 nm, respectively. The emission bands at 161, 175, 184 (partly), and 199 nm are assigned to the spin-allowed transitions from the low-spin $4f^{11}5d$ state (triplet state) to 3H_6 , 3F_4 , 3H_5 , and 3H_4 , respectively. Just as for Er^{3+} , the Stokes shifts for the $4f^{11}5d(\text{HS}) \rightarrow 4f^{12}(^3H_6)$ and $4f^{11}5d(\text{LS}) \rightarrow 4f^{12}(^3H_6)$ emissions are similar, in this case approximately $1.7 \times 10^3\text{ cm}^{-1}$.

Luminescence decay curves were recorded for the three highest-energetic $\text{Tm}^{3+}f-d$ emission bands. The curves for the 161- and 168-nm emissions are presented in Figs. 8(a) and 8(b), respectively. The emission at 161 nm decays single exponentially with a decay time of 16 ns. The same value was obtained for the $f-d$ emission band at 175 nm, showing that both emissions are spin allowed and originate from the triplet $4f^{11}5d$ state. As can be seen in Fig. 8(b), the decay curve of the 168-nm emission band decreases slightly within 1 μs , just as the curve of the 167-nm emission for Er^{3+} in LiYF_4 [Fig. 6(b)]. In contrast with Er^{3+} , the decay curve of this $f-d$ emission band of Tm^{3+} in LiYF_4 exhibits no initial rise. Indeed, there is no $4f^{12}$ level situated in between the two lowest $4f^{11}5d$ states, as there was for Er^{3+} in LiYF_4 . The only $4f^{12}$ level of Tm^{3+} in the VUV region is 1S_0 around $75\,000\text{ cm}^{-1}$, which is much higher than the lowest $4f^{11}5d$ states.³¹ Thus, the quintet $4f^{11}5d$ state is fed directly

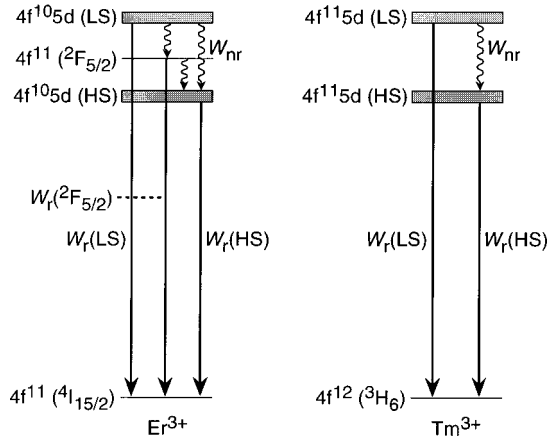


FIG. 9. Schematic energy level diagrams for Er^{3+} and Tm^{3+} in LiYF_4 , showing the radiative and nonradiative processes leading to various types of emission after f - d excitation.

by the nonradiative relaxation from the lowest triplet state, which is so fast [Fig. 8(a)] that this rise cannot be observed in Fig. 8(b). This difference between Tm^{3+} and Er^{3+} is schematically depicted in Fig. 9. The experimental decay curve in Fig. 8(b) could be fit to a single-exponential curve, which gave a decay time of 8 μs . This value shows that the assignment of the 168-nm emission to a spin-forbidden f - d transition is correct.

For both $\text{LiYF}_4:\text{Er}^{3+}$ [Fig. 3(a)] and $\text{LiYF}_4:\text{Tm}^{3+}$ (Fig. 7), it can be seen that for spin-forbidden as well as spin-allowed transitions the emission to the ground state is the strongest. The transitions to higher $4f^n$ levels are much weaker [except for spin-allowed emission for Tm^{3+} where the transition to the first excited $4f^{12}$ state (3F_4) is also strong]. However, there is a clear difference between Er^{3+} and Tm^{3+} in relative intensities of total emission from the low-spin and the high-spin $4f^{n-1}5d$ state. For Tm^{3+} the total spin-allowed f - d emission intensity relative to total spin-forbidden f - d emission intensity is much higher than for Er^{3+} . We have calculated the ratios of spin-forbidden to spin-allowed emission intensity, further denoted as $R(\text{HS/LS})_{em}$, from the f - d emission spectra. The values are given in Table I, together with the measured decay times. For Er^{3+} in LiYF_4 $R(\text{HS/LS})_{em}$ is approximately 11, whereas for Tm^{3+} $R(\text{HS/LS})_{em}$ is about 3, both at low temperature. Next to that, the low-temperature decay time mea-

sured for the spin-allowed emission of $\text{LiYF}_4:\text{Tm}^{3+}$ is much longer than that of $\text{LiYF}_4:\text{Er}^{3+}$ (16 vs 4.5 ns, see Table I). These differences can be explained by the presence of the ${}^2F(2)_{5/2}$ level for Er^{3+} in between the high-spin and low-spin $4f^{10}5d$ states. This is clarified using the energy level diagram in Fig. 9, which schematically shows the processes that occur upon excitation in the low-spin $4f^{n-1}5d$ states for Er^{3+} and Tm^{3+} . The $4f^{n-1}5d$ states are given as broad horizontal bars to distinguish them from $4f^n$ levels (narrow horizontal bars). Radiative and nonradiative transitions are shown as straight and wavy arrows, respectively. For simplicity emission is drawn as an arrow to the $4f^n$ ground state, although emission to the other $4f^n$ levels also occurs. For Tm^{3+} , from the low-spin $4f^{11}5d$ state two processes occur: radiative decay to the various $4f^{12}$ states and nonradiative decay to the high-spin $4f^{11}5d$ state, with probabilities $W_r(\text{LS})$ and W_{nr} , respectively. From the high-spin $4f^{11}5d$ state only radiative decay takes place, with probability $W_r(\text{HS})$. Thus, the competition between radiative and nonradiative decay from the low-spin state determines the relative intensities of spin-allowed and spin-forbidden f - d emission. For Er^{3+} , the presence of the ${}^2F(2)_{5/2}$ level allows for nonradiative decay from the low-spin $4f^{10}5d$ state to the high-spin state in two steps, via the ${}^2F(2)_{5/2}$ level. From the high-spin state only radiative decay occurs as the energy gap to the next lower $4f^{11}$ level [${}^2D(2)_{3/2}$] is some 5000 cm^{-1} .²⁷ Evidence for nonradiative relaxation from the low-spin $4f^{10}5d$ state via the ${}^2F(2)_{5/2}$ state is the observation of weak ${}^2F(2)_{5/2}$ emission lines. The ${}^2F(2)_{5/2}$ emissions, of which the strongest lie in the UV,²⁷ are very weak relative to spin-forbidden f - d emission. Therefore, in approximation $R(\text{HS/LS})_{em}$ is directly determined by the competition between radiative and nonradiative decay from the low-spin $4f^{10}5d$ state, just as for Tm^{3+} . With this information the radiative and nonradiative decay rates can be calculated. The intensity ratio of spin-forbidden to spin-allowed f - d emission is equal to:

$$R(\text{HS/LS})_{em} = \frac{W_{nr}}{W_r(\text{LS})}. \quad (1)$$

The measured decay time of the spin-allowed f - d emission $\tau(\text{LS})$ represents the total decay from the low-spin state,

$$\frac{1}{\tau(\text{LS})} = W_{\text{tot}}(\text{LS}) = W_r(\text{LS}) + W_{nr}. \quad (2)$$

TABLE I. f - d emission data for Er^{3+} and Tm^{3+} in LiYF_4 and YF_3 : measured decay times of spin-allowed f - d emission [$\tau(\text{LS})$] and spin-forbidden f - d emission [$\tau_r(\text{HS})$], ratios of spin-forbidden to spin-allowed f - d emission intensity [$R(\text{HS/LS})_{em}$], and calculated radiative decay times of spin-allowed f - d emission [$\tau_r(\text{LS})$]. The experimental error is some 10%, except for $\tau_r(\text{HS})$ ($\sim 20\%$). [n.m.] denotes: not measured.

	$\tau(\text{LS})$ (ns)		$(\text{HS/LS})_{em}$		$\tau_r(\text{LS})$ (ns)	$\tau_r(\text{HS})$ (μs)
	at 10 K	at 300 K	at 10 K	at 300 K		
$\text{LiYF}_4:\text{Er}^{3+}$	4.5	4.5	11	15	60	3
$\text{LiYF}_4:\text{Tm}^{3+}$	16	9	3	5	60	8
$\text{YF}_3:\text{Er}^{3+}$	5.5	0.6	6	>50	40	[n.m.]
$\text{YF}_3:\text{Tm}^{3+}$	22	9	2	8	70	[n.m.]

By substituting Eq. (1) in Eq. (2) $W_r(\text{LS})$ and W_{nr} can be calculated

$$W_r(\text{LS}) = \frac{1}{R(\text{HS/LS})_{em} + 1} \cdot \frac{1}{\tau(\text{LS})}, \quad (3)$$

$$W_{nr} = \frac{R(\text{HS/LS})_{em}}{R(\text{HS/LS})_{em} + 1} \cdot \frac{1}{\tau(\text{LS})}. \quad (4)$$

For $\text{LiYF}_4:\text{Er}^{3+}$ at low temperature, $W_{\text{tot}}(\text{LS}) = 2.2 \times 10^8 \text{ s}^{-1}$, so the values calculated for $W_r(\text{LS})$ and W_{nr} are $1.9 \times 10^7 \text{ s}^{-1}$ and $2.0 \times 10^8 \text{ s}^{-1}$, respectively. In the same way, for Tm^{3+} $W_{\text{tot}}(\text{LS}) = 6.3 \times 10^7 \text{ s}^{-1}$, giving $W_r(\text{LS}) = 1.6 \times 10^7 \text{ s}^{-1}$ and $W_{nr} = 4.7 \times 10^7 \text{ s}^{-1}$. $W_r(\text{LS})$ for Er^{3+} and Tm^{3+} are similar, as expected. From $W_r(\text{LS})$ the radiative decay time of the spin-allowed $f-d$ emission $\tau_r(\text{LS})$ is estimated to be some 60 ns, which is also included in Table I. W_{nr} is much larger for Er^{3+} than for Tm^{3+} as the energy gap that has to be bridged to the next lower level [the ${}^2F(2)_{5/2}$ level and the high-spin $4f^{11}5d$ state, respectively] is much smaller for Er^{3+} . This explains why $R(\text{HS/LS})_{em}$ is higher for Er^{3+} compared with Tm^{3+} , and the shorter decay time of the spin-allowed $f-d$ emission $\tau(\text{LS})$ for Er^{3+} .

Emission spectra and luminescence decay curves for Er^{3+} and Tm^{3+} in LiYF_4 were also recorded at room temperature (not shown). The decay times of the spin-allowed $f-d$ emission and the $R(\text{HS/LS})_{em}$ values found are included in Table I. For both samples the intensity of spin-forbidden $f-d$ emission relative to the spin-allowed emission has increased compared with the spectra at 10 K. The relative increase is stronger for Tm^{3+} , where $R(\text{HS/LS})_{em}$ goes from 3 to 5, than for Er^{3+} , where $R(\text{HS/LS})_{em}$ changes from 11 to 15. The decay time of the $f-d$ emission from the low-spin state has shortened for Tm^{3+} , whereas for Er^{3+} it has not changed significantly. Through the same procedure as was followed for the low-temperature measurements, the following values for $W_r(\text{LS})$ and W_{nr} are calculated: $1.4 \times 10^7 \text{ s}^{-1}$ and $2.1 \times 10^8 \text{ s}^{-1}$ respectively for Er^{3+} , and $2 \times 10^7 \text{ s}^{-1}$ and $9 \times 10^7 \text{ s}^{-1}$, respectively for Tm^{3+} . As expected, the radiative decay rate is not dependent on temperature. The larger increase for the nonradiative decay rate for Tm^{3+} compared with Er^{3+} can be understood from the fact that for Tm^{3+} the nonradiative relaxation involves one gap of about $2 \times 10^3 \text{ cm}^{-1}$ that can be bridged by 4 phonons [The maximum phonon energy in LiYF_4 is about 560 cm^{-1} (Ref. 32)]. For Er^{3+} nonradiative relaxation occurs in two steps of $1 \times 10^3 \text{ cm}^{-1}$, each involving 2 phonons. Since W_{nr} is proportional to $(n+1)^p$, n being the phonon occupation number and p the number of phonons involved,³³ the stronger temperature dependence is indeed expected for the higher order process.

The same observation of two kinds of emission for Er^{3+} and Tm^{3+} in LiYF_4 as described here was reported very recently.¹⁸ Similar VUV emission spectra and luminescence decay times in the same order of magnitude were found. The interpretation in Ref. 18 is different: the slow emission (μs decay time) was assigned to a parity-forbidden $f-f$ emission. It was not specified which high-lying $4f^n$ levels were involved. As was described above, for Tm^{3+} there are no $4f^{12}$ energy levels in this region, and for Er^{3+} the high-lying $4f^{11}$ levels were studied by us and found not to cause the emis-

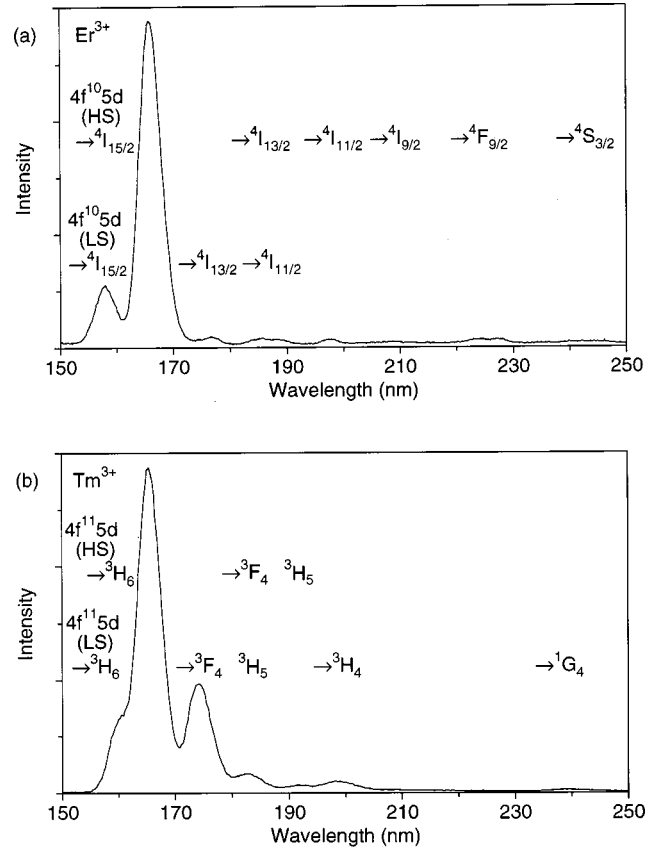


FIG. 10. (a) Emission spectrum of $\text{YF}_3:\text{Er}^{3+}$ 1% upon $4f^{11}({}^4I_{15/2}) \rightarrow 4f^{10}5d$ excitation (136 nm) at 11 K. (b) Emission spectrum of $\text{YF}_3:\text{Tm}^{3+}$ 1% upon $4f^{12}({}^3H_6) \rightarrow 4f^{11}5d$ excitation (141 nm) at 10 K.

sion bands which we assign to spin-forbidden $f-d$ emission. Next to that, the emission bands are broader than emissions we observed originating from $4f^{11}$ levels like ${}^2F(2)_{5/2}$. This provides evidence that the slow component of the VUV emission in $\text{LiYF}_4:\text{Er}^{3+}$ and $\text{LiYF}_4:\text{Tm}^{3+}$ is spin-forbidden $f-d$ emission and not $f-f$ emission.

Er^{3+} and Tm^{3+} are the only heavy lanthanides for which $f-d$ emission takes place. The other lanthanides with a more than half-filled $4f$ shell for which a spin-forbidden $f-d$ transition was observed in excitation (Tb^{3+} , Dy^{3+} , and Ho^{3+}) have $4f^n$ levels just below the high-spin $4f^{n-1}5d$ state and in between the high-spin and lowest low-spin state. As a consequence, nonradiative decay followed by $f-f$ emission occurs and neither spin-allowed nor spin-forbidden $f-d$ emission can be observed.

3.3. $f-d$ emission for Er^{3+} and Tm^{3+} in other fluorides

To investigate if spin-allowed and spin-forbidden $f-d$ emission can occur for other hosts than LiYF_4 , we have studied the $f-d$ transitions in $\text{YF}_3:\text{Er}^{3+}$, $\text{YF}_3:\text{Tm}^{3+}$, and $\text{LaF}_3:\text{Er}^{3+}$. The low-temperature emission spectra for powder samples of Er^{3+} and Tm^{3+} in YF_3 upon excitation into higher-lying low-spin $4f^{n-1}5d$ states are shown in Figs. 10(a) and 10(b), respectively. These spectra are similar to the emission spectra of Er^{3+} and Tm^{3+} in LiYF_4 [Figs. 3(a) and 7, respectively], regarding position as well as relative intensities of the various bands. Consequently, the emission bands are assigned in the same way as for LiYF_4 to transitions from

the high-spin and low-spin $4f^{n-1}5d$ state, as can be seen in Fig. 10. The bands at 166 and 158 nm for Er^{3+} and 166 and 160 nm for Tm^{3+} correspond to the spin-forbidden and spin-allowed $f-d$ transitions to the $4f^n$ ground state, respectively, and the remaining bands are due to $f-d$ transitions to $4f^n$ excited states. For Tm^{3+} the separation between the spin-allowed and spin-forbidden emission to 3H_6 (160 and 166 nm) is slightly smaller compared with LiYF_4 . It should be noted that some of the bands in the spectrum of $\text{YF}_3:\text{Er}^{3+}$ are partly due to ${}^2F(2)_{5/2}$ emission, which appears to be somewhat stronger in YF_3 than in LiYF_4 .²⁷

The luminescence decay curves (not shown) recorded for several emissions show that the emissions assigned to spin-allowed $f-d$ transitions are indeed fast, and emissions assigned to spin-forbidden transitions are relatively slow. Decay times of 5.5 and 22 ns were obtained for the spin-allowed emission at low temperature of Er^{3+} and Tm^{3+} in YF_3 , respectively (Table I). For the spin-forbidden $f-d$ emission no decay times could be determined, because decay curves were recorded in a time range of only 200 ns, in which no significant decay was observed. This is an indication that the decay time is at least some μs . These results confirm the assignment of the emissions in Fig. 10 to spin-allowed and spin-forbidden $f-d$ transitions. The $f-d$ excitation spectra recorded for Er^{3+} and Tm^{3+} in YF_3 (not shown) strongly resemble the spectra reported before.¹⁰ Just as for LiYF_4 , several strong broad bands are observed, which are assigned to excitations to low-spin $4f^{n-1}5d$ states, but no vibrational fine structure is present. The lowest spin-allowed $f-d$ excitation has its maximum at 147 nm for both Er^{3+} and Tm^{3+} . This is at higher energy than for LiYF_4 , which is due to the larger site for the lanthanide ion because of the higher coordination number (9 vs 8). As a consequence of the larger ion-ligand distance the crystal-field splitting decreases, causing a shift to higher energy of the lowest $4f^{n-1}5d$ level. For both Er^{3+} and Tm^{3+} in YF_3 , the transition to the high-spin $4f^{n-1}5d$ state could not be observed in excitation. The observation of a weak spin-forbidden $f-d$ band in the excitation spectrum can be more difficult in comparison with LiYF_4 due to the lack of fine structure.

As the $f-d$ excitations are at higher energies than in LiYF_4 while the emission bands are roughly at the same positions, the Stokes shifts are larger for YF_3 . For the transition between the ground state and the lowest low-spin $4f^{n-1}5d$ state the Stokes shift can be calculated to be approximately $4.7 \times 10^3 \text{ cm}^{-1}$ for Er^{3+} and $5.4 \times 10^3 \text{ cm}^{-1}$ for Tm^{3+} . The value of Tm^{3+} is somewhat higher than that of Er^{3+} , which was also found for LiYF_4 . The larger Stokes shift for YF_3 compared with LiYF_4 and the absence of fine structure indicate that the electron-lattice coupling is stronger than for LiYF_4 , causing a larger offset of the $4f^{n-1}5d$ states in the configuration coordinate model. In spite of this stronger coupling, the observation of spin-allowed emission shows that from the lowest low-spin state radiative decay can compete with nonradiative decay. The intensity of spin-allowed $f-d$ emission relative to spin-forbidden emission at low temperature is even stronger compared with LiYF_4 for both Er^{3+} and Tm^{3+} . This can be explained by the lower maximum phonon energy in YF_3 compared with LiYF_4 .³⁴ To bridge the gap of about $2 \times 10^3 \text{ cm}^{-1}$, some 6 phonons have

to be emitted for nonradiative decay in YF_3 , lowering its probability compared to the 4-phonon emission in LiYF_4 . The $R(\text{HS/LS})_{em}$ values for $\text{YF}_3:\text{Er}^{3+}$ and $\text{YF}_3:\text{Tm}^{3+}$ from the spectra in Fig. 10 are 6 and 2, respectively (Table I). From these values and the decay times of the spin-allowed emission, the following values for $W_r(\text{LS})$ and W_{nr} were calculated using Eqs. (3) and (4): $2.6 \times 10^7 \text{ s}^{-1}$ and $1.6 \times 10^8 \text{ s}^{-1}$ for Er^{3+} and $1.5 \times 10^7 \text{ s}^{-1}$ and $3.0 \times 10^7 \text{ s}^{-1}$ for Tm^{3+} , respectively. $W_r(\text{LS})$ and the corresponding radiative decay time $\tau_r(\text{LS})$, which is also given in Table I, is about the same as for LiYF_4 , whereas W_{nr} is smaller than in LiYF_4 for both Er^{3+} and Tm^{3+} . In accordance with the results for LiYF_4 , W_{nr} is much larger for $\text{YF}_3:\text{Er}^{3+}$ than for $\text{YF}_3:\text{Tm}^{3+}$, which is explained by relaxation via the ${}^2F(2)_{5/2}$ level for Er^{3+} .

The $f-d$ emission spectra of Er^{3+} and Tm^{3+} in YF_3 recorded at room temperature (not shown) show almost only spin-forbidden emission. The spin-allowed $f-d$ emission has nearly vanished, indicating that nonradiative decay from the low-spin to the high-spin state has become much more probable than at 10 K. Indeed, the decay times measured for the $f-d$ emission from the low-spin state are much shorter: 0.6 ns for Er^{3+} and 9 ns for Tm^{3+} (Table I). For $\text{YF}_3:\text{Tm}^{3+}$ $R(\text{HS/LS})_{em}$ was found to be about 8. The $R(\text{HS/LS})_{em}$ value for $\text{YF}_3:\text{Er}^{3+}$ could not be determined because of a too small intensity of spin-allowed $f-d$ emission relative to spin-forbidden emission; in other words, it is much larger than the other values given in this paper. The calculated values of $W_r(\text{LS})$ and W_{nr} for Tm^{3+} in YF_3 at room temperature are $1.2 \times 10^7 \text{ s}^{-1}$ and $1 \times 10^8 \text{ s}^{-1}$, respectively, showing that W_{nr} is much higher than at low temperature. The stronger increase of the nonradiative decay rate with temperature for YF_3 compared with LiYF_4 is explained qualitatively by the fact that more phonons are needed (see Sec. 3.2) and the stronger coupling with the lattice.

The emission spectrum of Er^{3+} in LaF_3 (not shown) is different. Upon excitation into the high $4f^{10}5d$ states a strong emission band at 161 nm and in addition many weaker and narrower bands at longer wavelength are observed, at low as well as room temperature. No emission is observed at shorter wavelength. In the VUV excitation spectrum broad bands corresponding to transitions to quartet $4f^{10}5d$ states are observed, of which the lowest has its maximum at approximately 145 nm. This is at higher energy than for $\text{YF}_3:\text{Er}^{3+}$, in accordance with the larger lanthanide site as La^{3+} is bigger than Y^{3+} (see above). At 150 nm a weak band is present, which is assigned to the $f-d$ transition to the sextet state. The 161-nm band in the emission spectrum is assigned to the transition from the high-spin $4f^{10}5d$ state to the ground state, resulting in a Stokes shift similar as was found for $\text{YF}_3:\text{Er}^{3+}$ ($4.5 \times 10^3 \text{ cm}^{-1}$). A decay time of 0.4 μs was measured at 10 K, supporting the assignment to spin-forbidden $f-d$ emission. The other bands correspond to ${}^2F(2)_{5/2}$ emissions ($\tau > 1 \mu\text{s}$), which are relatively strong because in this case the ${}^2F(2)_{5/2}$ level is situated just below the high-spin $4f^{10}5d$ state.²⁷ This implies that from the high-spin state nonradiative decay occurs, which explains that the decay time of the spin-forbidden $f-d$ emission is shorter than $\tau_r(\text{HS})$ for $\text{LiYF}_4:\text{Er}^{3+}$. No spin-allowed $f-d$ emission could be measured for Er^{3+} in LaF_3 , in contrast to LiYF_4 and

YF₃. Apparently, in LaF₃ the probability for nonradiative decay from the lowest quartet $4f^{10}5d$ state is much higher than the radiative decay probability.

The VUV emission spectra of some more Er³⁺ and Tm³⁺-doped fluoride compounds were reported in Ref. 18. For Er³⁺ and Tm³⁺ in BaY₂F₈ both slow (μ s) and fast (ns) emission were found, whereas for SrF₂:Er³⁺ only the slow component was observed. Based on the present results for the luminescence of Er³⁺ and Tm³⁺, the emissions can be assigned to spin-allowed (fast) and spin-forbidden (slow) f - d emission. In the spectra of ErF₃ and TmF₃, which have the same structure as YF₃, only the fast emission is present, at the same positions as the spin-allowed f - d emission for Er³⁺ and Tm³⁺ in YF₃ (Fig. 10). The spin-forbidden f - d emission seems to be absent due to concentration quenching, but it is beyond the scope of this paper to discuss that in detail. Summarizing, for heavy lanthanides it is dependent on the host lattice and the temperature whether both spin-allowed and spin-forbidden f - d emission occur, and in which ratio. Finally, we want to note that the spin-forbidden character of the emission from the lowest $4f^{n-1}5d$ state makes heavy lanthanides unsuitable for application in scintillators, which require a short (ns) decay time.⁶

IV. CONCLUSIONS

Results on the $4f^n \leftrightarrow 4f^{n-1}5d$ spectroscopy of heavy trivalent lanthanides ($n > 7$) are presented. High-resolution excitation spectra of LiYF₄ doped with Tb³⁺, Dy³⁺, Ho³⁺,

Er³⁺, and Tm³⁺ show several strong f - d bands exhibiting fine structure, and a weak f - d band at lower energy. The weak band is a spin-forbidden transition to a high-spin $4f^{n-1}5d$ state, which can be expected for all lanthanides with a more than half-filled $4f$ shell.

As a consequence of the high-spin $4f^{n-1}5d$ state, for Er³⁺ and Tm³⁺ two types of f - d emission occur: spin-forbidden emission from the high-spin state with a decay time of some μ s, and spin-allowed emission from the lowest low-spin state with a decay time of some ns. These two types of f - d emission are observed for Er³⁺ and Tm³⁺ in LiYF₄ as well as in other fluorides. The situation is analogous to the occurrence of fluorescence and phosphorescence in organic molecules.

ACKNOWLEDGMENTS

The authors are grateful to Dr. P. Gürtler from HASY-LAB for the opportunity to use the HIGITI experimental station at the DESY synchrotron, Hamburg (Germany), and to Professor H. U. Güdel (University of Bern, Switzerland) for helpful discussions. H. Donker, A. P. Vink, A. van Dijken, L. van Pieterse, K. D. Oskam, and M. Heeroma are acknowledged for their help in carrying out the measurements. The work described here was supported by the Council for Chemical Sciences (CW), with financial aid from the Netherlands Organization for Scientific Research (NWO) and the Netherlands Foundation for Technical Research (STW).

*Author to whom correspondence should be addressed. FAX: +31 30 2532403. Electronic address: R.T.Wegh@phys.uu.nl

¹C. R. Ronda, *J. Alloys Compd.* **225**, 534 (1995).

²G. Blasse and B. C. Grabmaier, *Luminescent Materials* (Springer Verlag, Berlin, 1994), p. 130.

³R. T. Wegh, H. Donker, A. Meijerink, R. J. Lamminmäki, and J. Hölsä, *Phys. Rev. B* **56**, 13 841 (1997).

⁴R. T. Wegh, H. Donker, K. D. Oskam, and A. Meijerink, *Science* **283**, 663 (1999).

⁵R. W. Waynant and P. H. Klein, *Appl. Phys. Lett.* **46**, 14 (1985).

⁶C. W. E. van Eijk, *Proc. SPIE* **2706**, 158 (1996).

⁷E. Loh, *Phys. Rev.* **147**, 332 (1966).

⁸L. R. Elias, Wm. S. Heaps, and W. M. Yen, *Phys. Rev. B* **8**, 4989 (1973); Wm. S. Heaps, L. R. Elias, and W. M. Yen, *ibid.* **13**, 94 (1976).

⁹T. Szczurek and M. Schlesinger, in *Proceedings of the International Symposium on Rare Earth Spectroscopy*, edited by B. Jeżowska-Trebiatowska, J. Legendziewicz, and W. Stręk (World Scientific, Singapore, 1985), p. 309.

¹⁰K. H. Yang and J. A. DeLuca, *Appl. Phys. Lett.* **29**, 499 (1976); *Phys. Rev. B* **17**, 4246 (1978).

¹¹L. I. Devyatkova, O. N. Ivanova, V. V. Mikhailin, S. N. Rudnev, B. P. Uvarova, and S. P. Chernov, *Dokl. Akad. Nauk SSSR* **283**, 1339 (1985) [*Sov. Phys. Dokl.* **30**, 687 (1985)].

¹²K. M. Devyatkova, O. N. Ivanova, K. B. Seiranyan, S. A. Tamazyan, and S. P. Chernov, *Dokl. Akad. Nauk SSSR* **310**, 72 (1990) [*Sov. Phys. Dokl.* **35**, 40 (1990)].

¹³K. M. Devyatkova, O. N. Ivanova, S. A. Oganessian, K. B. Seiranyan, and S. P. Chernov, *Dokl. Akad. Nauk SSSR* **310**, 577 (1990) [*Sov. Phys. Dokl.* **35**, 56 (1990)].

¹⁴E. Sarantopoulou, A. C. Cefalas, M. A. Dubinskii, C. A. Nicolaidis, R. Yu. Abdulsabirov, S. L. Korableva, A. K. Naumov, and V. V. Semashko, *Opt. Commun.* **107**, 104 (1994).

¹⁵E. Sarantopoulou, A. C. Cefalas, M. A. Dubinskii, Z. Kollia, C. A. Nicolaidis, R. Yu. Abdulsabirov, S. L. Korableva, A. K. Naumov, and V. V. Semashko, *J. Mod. Opt.* **41**, 767 (1994).

¹⁶E. Sarantopoulou, Z. Kollia, A. C. Cefalas, M. A. Dubinskii, C. A. Nicolaidis, R. Yu. Abdulsabirov, S. L. Korableva, A. K. Naumov, and V. V. Semashko, *Appl. Phys. Lett.* **65**, 813 (1994).

¹⁷J. C. Krupa and M. Queffelec, *J. Alloys Compd.* **250**, 287 (1997).

¹⁸J. Becker, J. Y. Gesland, N. Yu. Kirikova, J. C. Krupa, V. N. Makhov, M. Runne, M. Queffelec, T. V. Uvarova, and G. Zimmerer, *J. Lumin.* **78**, 91 (1998).

¹⁹C. K. Jørgensen and J. S. Brinen, *Mol. Phys.* **6**, 629 (1963).

²⁰T. Hoshina and S. Kuboniwa, *J. Phys. Soc. Jpn.* **31**, 828 (1971); **32**, 771 (1972).

²¹L. J. Nugent, R. D. Baybarz, J. L. Burnett, and J. L. Ryan, *J. Phys. Chem.* **77**, 1528 (1973).

²²R. T. Wegh, H. Donker, and A. Meijerink, *Phys. Rev. B* **57**, R2025 (1998).

²³M. Robinson, *J. Cryst. Growth* **75**, 184 (1986).

²⁴R. E. Thoma, C. F. Weaver, H. A. Friedman, H. Insley, L. A. Harris, and H. A. Yakel, *J. Phys. Chem.* **65**, 1096 (1961).

²⁵A. Zalkin and D. H. Templeton, *J. Am. Chem. Soc.* **75**, 2453 (1953).

²⁶H. S. Kiliaan, A. Meijerink, and G. Blasse, *J. Lumin.* **35**, 155 (1986).

²⁷R. T. Wegh and A. Meijerink (unpublished).

²⁸G. Blasse, *J. Phys. Chem. Solids* **50**, 99 (1989).

- ²⁹C. de Mello Donegá, A. Meijerink, and G. Blasse, *J. Lumin.* **62**, 189 (1994).
- ³⁰D. J. Ehrlich, P. F. Moulton, and R. M. Osgood, Jr., *Opt. Lett.* **4**, 184 (1979).
- ³¹W. T. Carnall, G. L. Goodman, K. Rajnak, and R. S. Rana, Argonne National Laboratory Report No. ANL-88-8, 1988 (unpublished), p. 114.
- ³²S. A. Miller, H. E. Rast, and H. H. Caspers, *J. Chem. Phys.* **52**, 4172 (1970).
- ³³L. A. Riseberg and M. J. Weber, in *Progress in Optics XIV*, edited by E. Wolf (North-Holland, Amsterdam, 1976), p. 120.
- ³⁴G. Blasse, L. H. Brixner, and G. Hyatt, *Chem. Phys. Lett.* **164**, 617 (1989).